An Experimental Study of Critical Heat Flux in Non-uniformly Heated Vertical Annulus under Low Flow Conditions

Se-Young Chun*, Sang-Ki Moon, Won-Pil Baek, Moon-Ki Chung
Korea Atomic Energy Research Institute, 150 Dukjin-dong, Yusong-gu, Daejon 305-353, Korea
Masanori Aritomi
Research Laboratory for Nuclear Reactor, Tokyo Institute of Technology, 2-12-1 Ohokayama, Megro-ku, Tokyo 152, Japan

An experimental study on critical heat flux (CHF) has been performed in an internally heated vertical annulus with non-uniform heating. The CHF data for the chopped cosine heat flux have been compared with those for uniform heat flux obtained from the previous study of the authors, in order to investigate the effect of axial heat flux distribution on CHF. The local CHF with the parameters such as mass flux and critical quality shows an irregular behavior. However, the *total critical power* with mass flux and the *average CHF* with critical quality are represented by a unique curve without the irregularity. The effect of the heat flux distribution on CHF is large at low pressure conditions but becomes rapidly smaller as the pressure increases. The relationship between the critical quality and the boiling length is represented by a single curve, independent of the axial heat flux distribution. For non-uniform axial heat flux distribution, the prediction results from Doerffer et al.'s and Bowring's CHF correlations have considerably large errors, compared to the prediction for uniform heat flux distribution.

Key Words: Critical Heat Flux, Heated Vertical Annulus, Low Mass Flux, Wide Range Pressure, Non-uniform Heating, Effect of Axial Heat Flux Distribution, Boiling Length

Nomenclature

A_f : Cross sectional flow area [m^2]
$A_{CHF,h}$: Heated area from the bottom end of the heated section to CHF occurrence location [m^2]
d_i : Diameter of heater rod [m]
d_o : Inner diameter of outer pipe in annulus test section [m]
G : Mass flux [kg/m^2s]
G^* : Dimensionless mass flux, defined by Eq. (1) [−]
g : Gravitational acceleration [m/s^2]
h_{lg} : Latent heat of evaporation [kJ/kg]
$L_{CHF,B}$: Length from the onset of saturated boiling to the CHF occurrence location [m]
L_h : Heated length [m]
N : Total number of data
P : Pressure [MPa]
Q_{CHF} : Power supplied to the heated section at CHF occurrence [kW]
$Q_{CHF,loc}$: *Local critical power*, defined as the total power from the bottom end of the heated section to the CHF occurrence location [kW]
$Q_{CHF,T}$: *Total critical power*, defined as the total power supplied to the heated section at CHF occurrence [kW]
Q_T : Total power supplied to the heated section [kW]
q^*_{CHF} : Dimensionless CHF, defined by Eq. (1) [−]

* Corresponding Author,
E-mail : sychun@kaeri.re.kr
TEL : +82-42-868-2948; **FAX** : +82-42-868-8362
Korea Atomic Energy Research Institute, 150 Dukjin-dong, Yusong-gu, Daejon 305-353, Korea. (Manuscript **Received** August 12, 2002; **Revised** May 9, 2003)

q'' : Heat flux [kW/m^2]
q''_{avg} : Average heat flux over the heated section [kW/m^2]
q''_{CHF} : Critical heat flux [kW/m^2]
$q''_{CHF,avg}$: *Average CHF*, defined as the average heat flux from the bottom end of the heated section to the CHF occurrence location [kW/m^2]
$q''_{CHF,avg,B}$: Average heat flux from onset of saturated boiling to the CHF occurrence location [kW/m^2]
$q''_{CHF,loc}$: *Local CHF*, defined as the heat flux at the CHF occurrence location [kW/m^2]
x : Thermodynamic equilibrium quality [−]
x_{CHF} : Critical quality, i.e., local quality at CHF occurrence location [−]
Z : Distance from the bottom end of the heated section [m]

Greek symbols

Δh_{in} : Inlet subcooling enthalpy [kJ/kg]
$\Delta\rho$: Density difference between saturated water and steam, $\rho_l-\rho_g$ [kg/m^3]
λ : Length scale of the Taylor wave, $\sqrt{\sigma/(g\Delta\rho)}$ [m]
ρ : Density [kg/m^3]
σ : Surface tension [N/m]

Subscripts

cor : Correlation
exp : Experiment
g : Vapor phase
l : Liquid phase
NU : Non-uniform heat flux distribution
U : Uniform heat flux distribution

1. Introduction

Critical heat flux (CHF) is one of the most important thermal hydraulic parameters limiting the thermal performance of water cooled nuclear reactors, because an inordinate rise of the reactor fuel surface temperature under CHF conditions is sometimes sufficient to cause melting of the fuel materials. The CHF behavior under low flow conditions is of much importance not only for accident analysis of the conventional nuclear reactors but also for a future advanced water cooled reactor, which will adapt to any passive safety feature such as natural circulation or low flow heat removal system. However, a deep understanding for the CHF under low flow conditions has not been acquired.

The experimental studies on low flow CHF were recently done (Mishima and Ishii, 1982; Rogers et al., 1982; El-Genk et al., 1988; Schoesse et al., 1997; Park et al., 1997). These studies were conducted in the test sections near atmospheric pressure conditions. The authors performed the CHF experiments in an internally heated annulus under low flow conditions over the pressure range of 0.57~15.01 MPa and discussed the effect of pressure on CHF (Chun et al., 2000 and 2001). The experimental efforts in previous studies on low flow CHF were made for the test section having a uniform axial heat flux distribution. The CHF data obtained in the test section with uniform heating, however, are not directly applicable to nuclear reactors since their heat flux distributions are inherently non-uniform axially.

Review of the literature on the effect of axial heat flux distribution on CHF indicates that there are basically three approaches in the prediction of CHF for a heated section with non-uniform axial heat flux distribution, that is, the 'overall power' hypothesis, the 'local conditions' hypothesis and the 'correction-factor' methods are currently popular. The 'overall power' hypothesis assumes that the total power which can be fed to the heated section with non-uniform heating will be the same as that for a uniformly heated section of the same geometry and heated length, with the same inlet conditions. This approach does not permit the prediction of location of the CHF and hence is not useful for nuclear reactor accident analysis. The 'local conditions' hypothesis assumes that the CHF is a function of only local thermal hydraulic conditions. This approach does not consider the effect of non-uniform upstream axial heat flux distribution on the CHF. These two approaches, as pointed out by Todreas and Rohsenow (1966), are valid only in the limited conditions and gen-

erally inadequate. The common observation in the literature is that the effect of axial heat flux distribution is strongly dependent on the CHF mechanisms. DNB (Departure from Nucleate Boiling) in the negative quality region is scarcely influenced by the upstream axial heat flux distribution and the effect of upstream heat flux distribution on DNB begins to appear as the quality increases. Liquid film dryout in the high quality region is strongly influenced by the upstream axial heat flux distribution.

The limitation of the 'overall power' and 'local conditions' hypotheses for predicting CHF in a heated section with non-uniform axial heat flux distribution led to some 'correction-factor' methods, which are usually built into the CHF correlation with the local condition form. Tong et al. (1965) proposed the method to predict CHF for the non-uniform heat flux distribution by using the F-factor defined as the ratio of the CHF at any given local enthalpy for the uniform heat flux distribution to the CHF at the same given local enthalpy for the non-uniform heat flux distribution. The form of the F-factor was obtained by considering an energy balance on the superheated boundary layer in the bubbly flow regime. The F-factor method is probably the best approach for the prediction of DNB heat flux in low quality region (Tong, 1966; Rosal et al., 1974). Bowring (1977) introduced the Y-parameter, which is defined as the ratio of the average heat flux from inlet of the heated section to the CHF location to the local heat flux at the CHF location, and incorporated this parameter into his CHF correlation. Groeneveld et al. (1986) used the ratio of the boiling length average heat flux (i.e., from the saturation point to the CHF location) to the local heat flux at the CHF location as an axial heat flux correction factor of the AECL-UO (Atomic Energy of Canada Research Company Ltd. -University of Ottawa) CHF look-up table, which was developed based on the uniform heat flux data.

In order to investigate the effect of axial heat flux distribution on CHF, the series of CHF experiments have been performed using the test section with non-uniform heating at the same geometry and flow conditions as the uniform heat flux experiments in the previous study of the authors. This paper provides the results obtained from the non-uniform heat flux experiments. The non-uniform heat flux data are compared with the CHF data from the uniform heat flux experiments, and the prediction performance of the existing CHF correlations for the test section with non-uniform heating is examined.

2. Experimental Descriptions

2.1 Test section

A description of the experimental facility can be found in references (Chun et al., 2000 and 2001). The test section used in this experimental work is described here in detail. The test section has the same geometry as that used in the uniform heat flux experiments in the previous studies. The heater rod with non-uniform axial heat flux distribution is used in the present experiments. Figure 1 shows the test section geometry and the locations of measuring sensors. The annulus flow channel consists of an outer pipe with an inner diameter of 19.4 mm and an inner heater rod with an outer diameter of 9.53 mm, having a heated length of 1842 mm at room temperature. The inner heater rod is heated indirectly by electricity. The sheath and heating element of the heater rod are made of Inconel 600 and Nichrome, respectively. Aluminum oxide and boron nitride are packed for the electric insulations inside the heating element and between the heating element and the sheath, respectively. For measuring the heater rod surface temperature and detecting the CHF occurrence, six Chromel-Alumel thermocouples (T/C 1~6 in Fig. 1) with a sheath outer diameter of 0.5 mm are embedded in the grooves hollowed out in the axial direction on the outer surface of the heater rod. The ratio of the local heat flux $q''(z)$ to the average heat flux q''_{avg} over the heated section is shown as a function of axial location of the heated section in Fig. 2. The heat flux level in the heated section is divided into 10 steps with a minimum and maximum heat flux ratio of 0.448 and 1.400, respectively, to simulate a symmetric chopped cosine heat flux profile. The

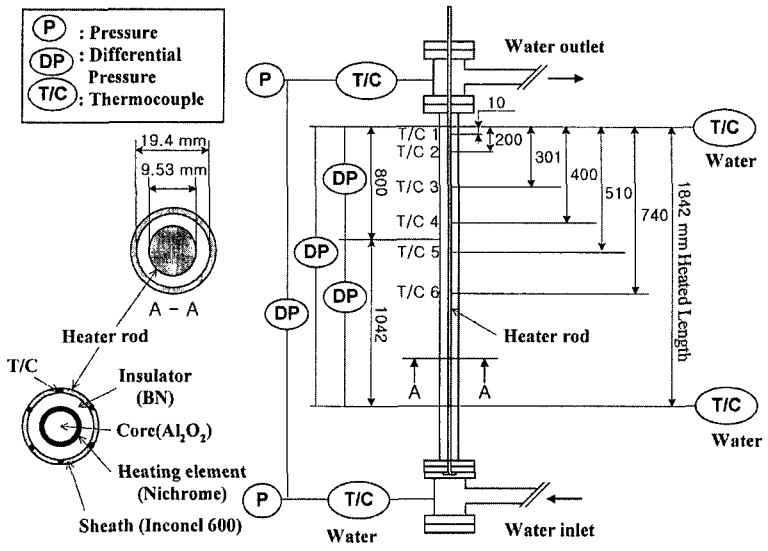

Fig. 1 Geometry and the locations of measuring sensors in the test section with non-uniform axial heat flux distribution

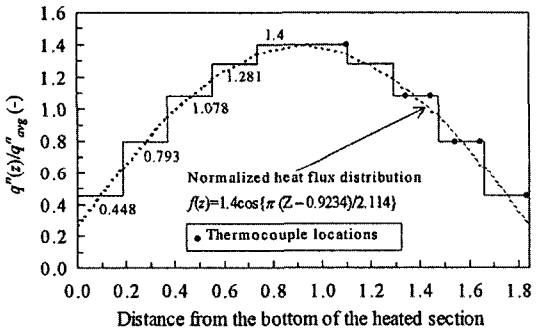

Fig. 2 Heat flux distribution of the heated section

axial power distribution is obtained by variations in the axial local electric resistance of the heating element. The temperature sensing points on the heater rod surface are located at 10, 200, 301, 400, 510 and 740 mm from the top end of the heated section.

2.2 Experimental procedure and conditions

The CHF experiments have been performed by the following procedure. First, the flow rate, inlet subcooling and system pressure are established at desired levels, power is then applied to the heater rod of the test section and increased gradually in small steps while the inlet conditions of the test section are kept at constant values. The period between the power steps is chosen as to be sufficiently long enough so that the loop can be stabilized at steady state conditions. This process continues until a sharp increase in temperature is observed in the heater rod surface. As the loop approaches CHF conditions, the temperature fluctuations of the heater rod surface are detected near the top of the heated section. The CHF conditions in the present experiments is determined when one of the surface temperatures of the heater rod rises continuously and then becomes 100 K higher than the saturated water temperature. Whenever the CHF is detected, the heater power is automatically reduced or tripped to prevent any damage to the heater rod.

In this work, a total of 290 CHF data was obtained. The experimental conditions under which the present data have been collected are as follows :

- system pressure	0.57～15.01 MPa
- mass flux	201～650 kg/m^{2}s
- inlet subcooling	86～353 kJ/kg
- critical quality	0.018～0.536

The pressure at the inlet plenum is specified as the system pressure. The inlet subcooling, which is defined as the enthalpy difference between saturated water and subcooling water in the inlet of the heated section, is determined from the water

temperature at the bottom end of the heated section and the pressure at the inlet plenum. The critical quality is the thermodynamic equilibrium quality at CHF occurrence location. The uncertainties of the measuring system have been estimated from the calibration of sensors and the accuracy of the equipment, according to a propagation error analysis based on Taylor's series method (ANSI/ASME PTC 19.1, 1985). The evaluated maximum uncertainties of pressure and temperature are less than ±0.3% and ±0.7 K of the readings in the range of interest, respectively. The uncertainties of the power supplied to the heater rod are always less than ±1.8% of the readings. The heat loss in the heated section should be taken into account in the calculation of the heat flux. The heat loss has been estimated by the pretests (i.e., heat balance tests) for each pressure condition and was less than 2% of the power input. As can be seen from Figs. 1 and 2, the CHF occurrence locations determined in this experiment have some error, since the CHF is judged from the sharp temperature rise that is detected by the thermocouples attached on the heater rod surface. Table 1 shows the errors of the CHF location and the *local critical power*, which is defined as the total power from the bottom end of the heated section to the CHF location in this paper.

Table 1 Error of the CHF location and *local critical power*

Thermocouple	Error	
	CHF location (mm)	*Local critical power* (%)
T/C 1	+10	+0.2
	−95	−2.1
T/C 2	+95	+3.2
	−50	−2.1
T/C 3	+50	+2.5
	−50	−2.6
T/C 4	+50	+3.0
	−55	−3.6
T/C 5	+55	+4.2
	−115	−9.5
T/C 6	+115	+12.9

3. Experimental Results and Discussions

3.1 Characteristics of CHF with non-uniform heating

The CHF for axially uniform heating usually occurs at the top end of the heated section. It is known that for a test section having a cosine heat flux distribution, the location of CHF occurrence is between the middle and the top end of the heated section (Collier and Thome, 1994). Figure 3 shows the locations of the CHF occurrence. In a few runs of the experiments, the temperatures monitored by two thermocouples (T/C 2 and 3) rose sharply at the same time under CHF conditions. In this case, the data are plotted at the middle location between two thermocouples in Fig. 3. The locations where the CHF takes place are mainly distributed at the thermocouples T/C 2 and 3, which are attached at the upstream location near the top end of the heated section. However, the CHFs frequently occur at the locations of T/C 4, 5 and 6 in the low pressure region below 2 MPa, and at the top end (T/C 1) of the heated section in the pressures higher than 10 MPa. Especially, most of the CHFs at a pressure of 0.57 MPa occur at the location of T/C 5. For mass fluxes of 201 to 351 kg/m^{2}s and pressures above 2 MPa, the CHF occurrence centers at the location of T/C 2. The effect of inlet subcooling on the location of CHF occurrence is not recognized in the present data.

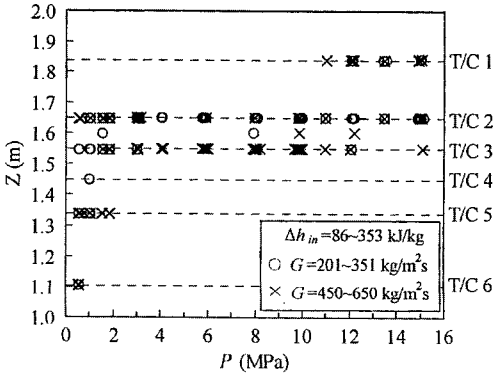

Fig. 3 Locations of CHF occurrence

The CHF characteristics are closely related to the two-phase flow pattern. In order to examine the two-phase flow pattern at the location where the CHF occurs, an approximate churn to annular flow transition boundary of Mishima and Nishihara (1987) is used. In Fig. 4, the present CHF data are plotted in terms of the dimensionless CHF q^*_{CHF} and mass flux G^*, and compared with the churn to annular flow transition boundary of Mishima and Nishihara. The dimensionless parameters are defined as follows:

$$q^*_{CHF}=Q_{CHF,loc,NU}/(A_{CHF,h}h_{lg}\sqrt{\lambda\rho_g g\Delta\rho})$$
$$G^*=G/\sqrt{\lambda\rho_g g\Delta\rho} \quad (1)$$
$$\lambda=\sqrt{\sigma/(g\Delta\rho)}$$

where $Q_{CHF,loc,NU}$ is the *local critical power*. The subscript '*NU*' denotes the non-uniform heat flux distribution. $A_{CHF,h}$ is the heated area from the bottom end of the heated section to the CHF location, h_{lg} the latent heat of evaporation, g the gravitational acceleration, G the mass flux, $\Delta\rho$ the difference between the liquid density ρ_l and vapor density ρ_g, λ the Taylor-wave length scale and σ the surface tension, respectively. The thermodynamic properties in Eq. (1) are determined from the pressure at the outlet plenum. As shown in the figure, the CHFs lie in the annular flow regime. The CHF occurs in an annular flow regime far from the churn flow regime as the inlet subcooling decreases (i.e., the quality at the location of CHF occurrence becomes higher.).

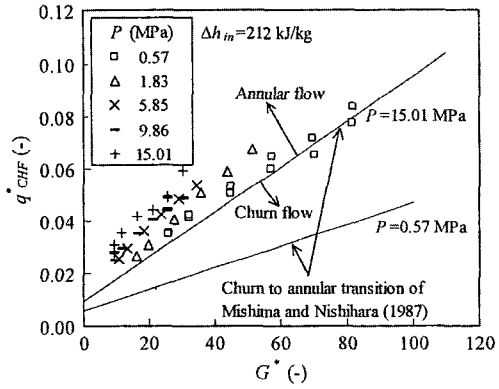

Fig. 4 Dimensionless CHF as a function of dimensionless mass flux for non-uniform heat flux data

Therefore, it is inferred that most of the CHFs in the present experiments occur due to dryout of the liquid film in annular flow.

Figure 5 shows *the local CHF* $q''_{CHF,loc,NU}$, which is defined as the heat flux at the location of the CHF occurrence, as a function of mass flux with the inlet subcooling as a parameter. The *local CHF* with the increasing mass flux shows an irregular behavior for the pressures of 0.57 and 15.01 MPa. On the other hand, the behavior of the *local CHF* under a pressure of 5.85 MPa shows a general trend, in which the CHF increases with increasing mass flux for a fixed inlet subcooling and increases with increasing inlet subcooling for a fixed mass flux. The CHFs mainly occur at the location of T/C 5 for a pressure of 0.57 MPa and at the location of T/C 2 for a pressure of 15.01 MPa. All the CHFs for a pressure of 5.85 MPa occur at the locations of T/C 2 and 3 having the same heat flux level. The *local CHF* data points to deviate from the linear relationship between the CHF and the mass flux

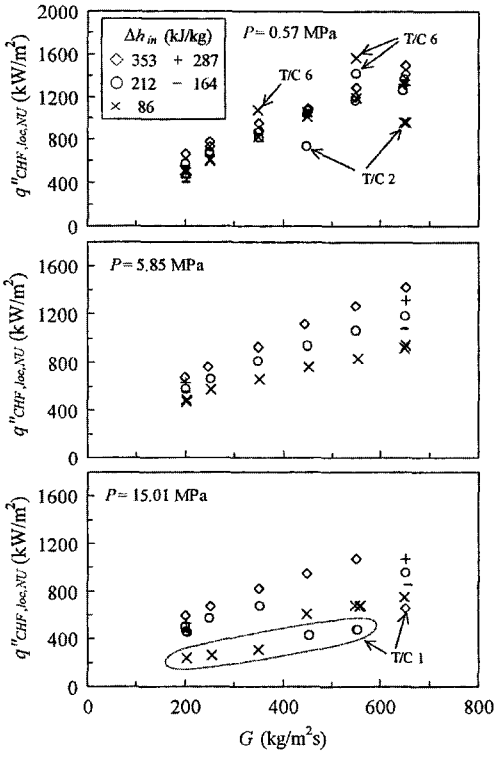

Fig. 5 Local CHF as a function of mass flux

in Fig. 5 correspond to the unsteady locations of the CHF occurrence. The total power supplied to the heated section at CHF occurrence, that is, the *total critical power* $Q_{CHF,T,NU}$ is shown as a function of mass flux in Fig. 6. The *total critical power* increases linearly with the increasing mass flux without the irregularity, in spite of the unsteadiness of the CHF occurrence location. The effect of inlet subcooling on the *total critical power* for a pressure of 0.57 MPa is smaller, compared with the *total critical power* data for the other pressures.

In Fig. 7, the *local CHFs* are plotted as a function of critical quality, from a viewpoint of the 'local conditions' hypothesis. A few data points deviate from a unique curve (approximately linear relationship in this case) of *local CHF* against critical quality due to the effect of CHF occurrence location. In the case of axial non-uniform heating, the effect of the upstream conditions on CHF is expected to be different from a uniform heating. If the location of CHF occurrence is in the high subcooled region, the CHF (i.e., in this case, the CHF mechanism is DNB.) is a local phenomenon and is then scarcely influenced by the upstream conditions. However, the CHF is usually considered that the upstream effect exists under normal flow conditions. In particular, the CHF in the high quality region, that is, liquid film dryout is strongly influenced by the upstream axial heat flux distribution. When the average heat flux from the bottom end of the heated section to the CHF occurrence location $q''_{CHF,avg,NU}$, which is referred to as the *average CHF* in this paper, is plotted as a function of critical quality, it is found that the *average CHF* and the critical quality can be approximately represented by a linear relationship as shown in Fig. 8. This linear relationship between the *average CHF* and the critical quality has been observed for the whole pressure range in the present experimental conditions. Figures 5~8 imply that the characteristics of the present CHF data cannot be represented with only local parameters and in addition to the

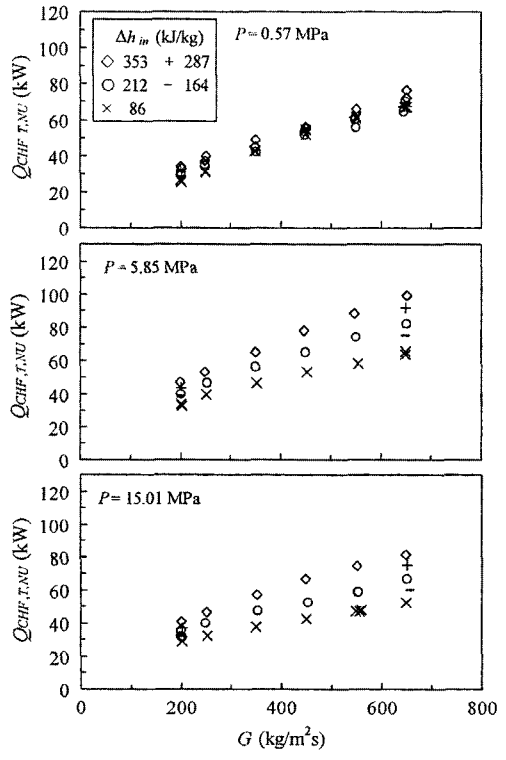

Fig. 6 *Total critical power* at CHF occurrence as a function of mass flux

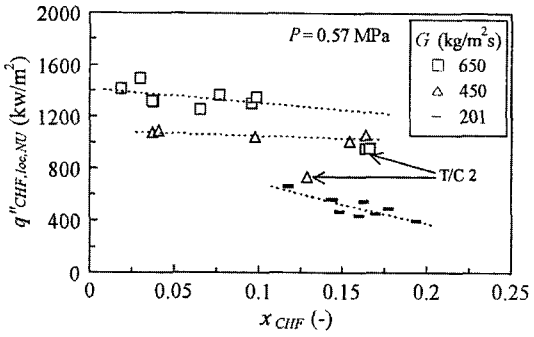

Fig. 7 *Local CHF* as a function of critical quality

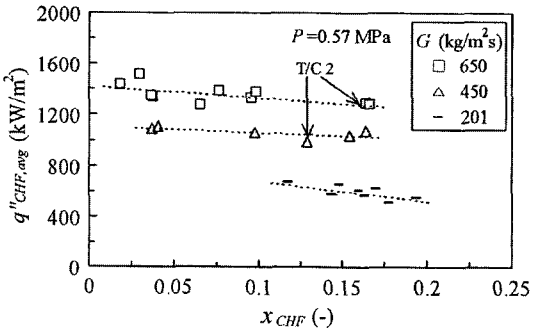

Fig. 8 *Average CHF* as a function of critical quality

local conditions, the integrated conditions over the heated section also are an important parameter.

In order to illustrate the effect of pressure on the CHF, the *local critical power* $Q_{CHF,loc,NU}$, *total critical power* $Q_{CHF,T,NU}$ and *average CHF* $q''_{CHF,avg,NU}$ are plotted as a function of pressure in Figs. 9~11, respectively. In Fig. 9, two peaks of the *local critical power* appear as the pressure increases for mass fluxes of 450~650 kg/m^{2}s. The *local critical power* increases irregularly as the pressure increases and then reaches the first peak value at about 2~4 MPa. Above this pressure, the *local critical power* decreases slowly with further increasing pressure, and presents a second peak value at 12 MPa. Figure 10 shows that, when the *total critical power* is plotted as a function of pressure, the *total critical power* increases rapidly up to about 2 MPa for mass fluxes of 450~650 kg/m^{2}s and has a gradual second peak at about 12~14 MPa for the mass fluxes of 550 and 650 kg/m^{2}s. The *average CHF* as a function of pressure is shown in Fig. 11. The *average*

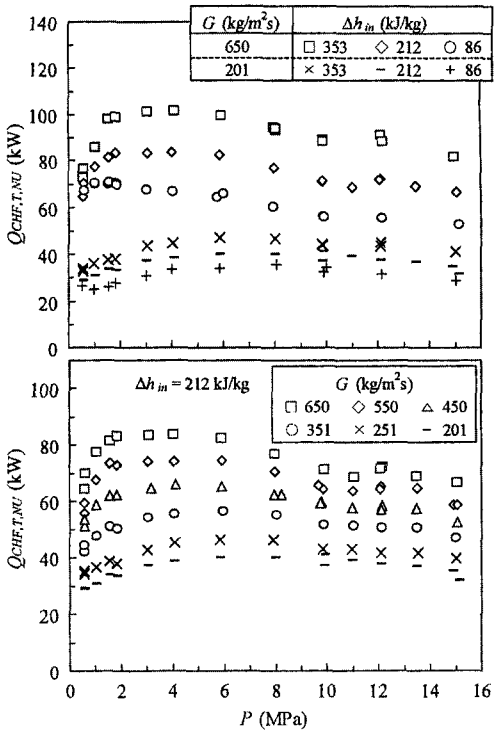

Fig. 10 Effect of pressure on *total critical power*

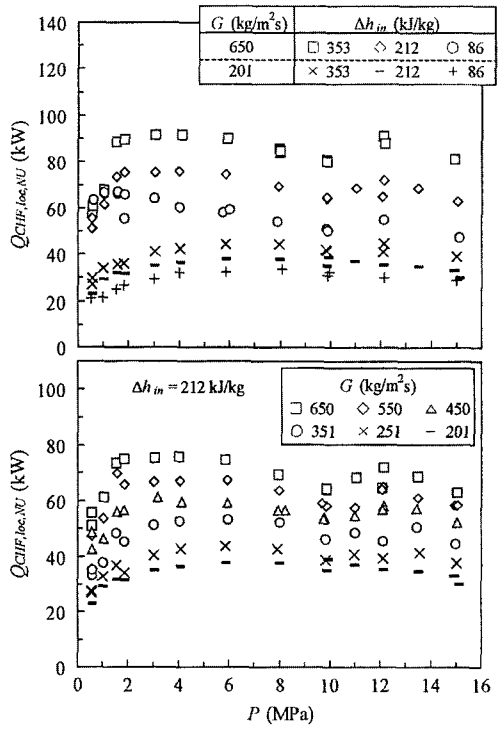

Fig. 9 Effect of pressure on *local critical power*

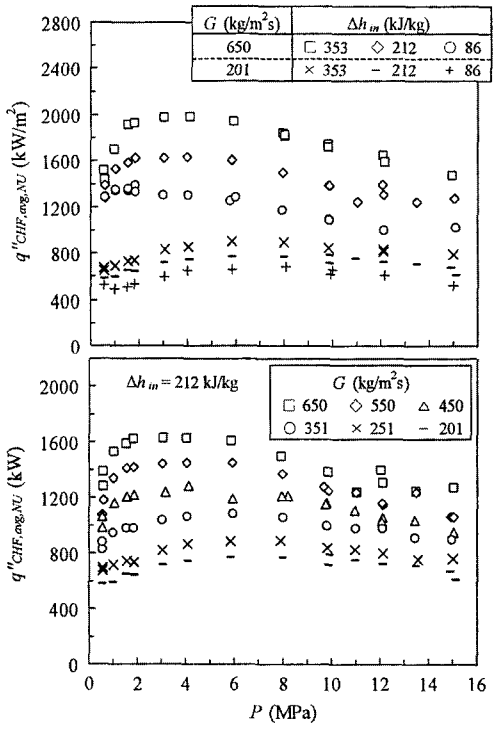

Fig. 11 Effect of pressure on *average CHF*

CHF does not have a clear second peak value for the variation of pressure. The existence of a second peak of the *local* and *total critical powers* in Figs. 9 and 10 results from the fact that the CHF can occur at the top end of the heated section at high pressures greater than 11 MPa as shown in Fig. 3. The effect of pressure on the CHF under low mass flux conditions is not so remarkable. The CHF behavior with pressure for the mass fluxes of 201 and 251 kg/m^{2}s shows the same trend as the CHF data obtained from the previous experiments (Chun et al., 2001) in the heated section with uniform heating.

3.2 Effect of axial heat flux distribution

The CHF experiments have been performed using the heater rod with the chopped cosine heat flux distribution under the same geometry and flow conditions as the uniform heat flux experiments in the previous studies (Chun et al., 2000 and 2001). The pairs of 231 data in the uniform and non-uniform heat flux have been obtained to investigate the effect of axial heat flux distribution on CHF. The flow conditions, that is, system pressures, mass fluxes and inlet subcoolings in each data pair cannot be set at the exactly same value. The average values of the absolute differences between two flow conditions in the uniform and non-uniform heat flux experiments are 0.039 MPa for system pressure, 2.5 kg/m^{2}s for mass flux and 4.8 kJ/kg for inlet subcooling.

For uniform heat flux distribution, the *local* CHF value is equal to the *average CHF* and the *local critical power* have the same value with the *total critical power* because the CHF occurs at the top end of the heated section. In this paper, for uniform heat flux distribution the *local* and *average CHFs* are designated by $q''_{CHF,U}$, the *local* and *total critical powers* by $Q_{CHF,U}$, respectively. The subscript 'U' denotes the uniform heat flux distribution. Figures 12~14 the *local critical power* ratio $Q_{CHF,U}/Q_{CHF,loc,NU}$, the *average CHF* ratio $q''_{CHF,U}/q''_{CHF,avg,NU}$ and the *total critical power* ratio $Q_{CHF,U}/Q_{CHF,T,NU}$ as a function of pressure, respectively. As shown in Fig. 12, most of the *local critical powers* for the non-uniform heat flux are lower than those for the uniform heat flux. The *local critical power* ratio shows a large scattering at low pressure conditions below 2 MPa. As the pressure increases, the scattering becomes rapidly smaller and the *local critical power* ratio has a tendency to gradually draw to a ratio of unity. On the other hand, when the *average CHF* ratio is plotted as a function of pressure (Fig. 13), though the scattering of the *average CHF* in the low pressure region decreases considerably, the *average CHFs* for the non-uniform heat flux are higher than those for the uniform heat flux in the pressures above 2 MPa. The behavior of the *total critical power* ratio in Fig. 14 supports the 'overall power' hypothesis. The values of the *total critical power* for the non-uniform heat flux agree with those for the uniform heat flux within an error of 10% at pressures above 2 MPa. The CHF correlation of the local condition type requires the critical quality. The

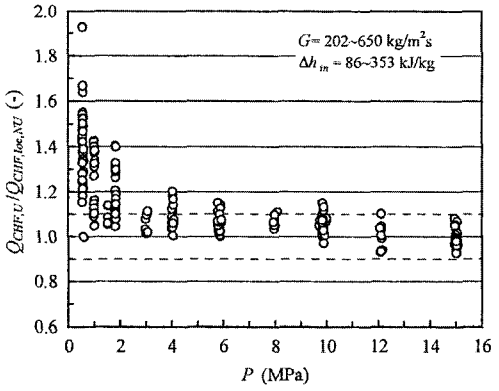

Fig. 12 *Local critical power* ratio with pressure

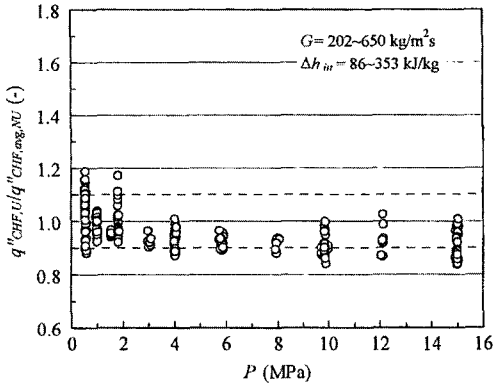

Fig. 13 *Average CHF* ratio with pressure

critical quality difference (i.e., $x_{CHF,U}-x_{CHF,NU}$) is shown as a function of pressure in Fig. 15. The critical qualities for the non-uniform heat flux are always lower than those for the uniform heat flux except for the high pressures of 12 and 15 MPa and a large scattering of the critical quality difference is observed at low pressure conditions below 2 MPa and at high pressure conditions above 10 MPa. A common feature in Fig. 12~15 is that the effect of the heat flux distribution on CHF is large at low pressure conditions below 2 MPa and the scattering of the CHF parameter ratios for the non-uniform and the uniform heat flux becomes rapidly smaller in the pressures above 2 MPa. Figures 12 and 15, in particular, show that the 'local conditions' hypothesis is not valid in the present experimental conditions and some integrated parameters over the heated section are required in order to predict the CHF with non-uniform heating.

A few experimental studies have reported that the relationship between boiling length and critical quality can fit both non-uniform and uniform heat flux data for qualities above 10% (Bergles et al., 1981). In Figs. 16(a) and (b), the critical quality is plotted as a function of boiling length $L_{CHF,B}$, which is defined as the axial distance from the saturation point to the CHF location. For a fixed mass flux and pressure, it is found from these figures that the relationship between the critical quality and the boiling length is represented by a single curve, independent of the axial heat flux distribution. The relationship of the critical quality and the boiling length in Fig. 16 can be presented as follows:

$$x_{CHF}=\frac{q''_{CHF,avg,B}\pi d_i L_{CHF,B}}{GA_f h_{lg}} \tag{2}$$

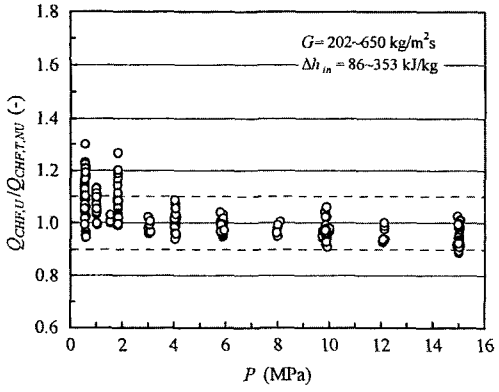

Fig. 14 *Total critical power* ratio with pressure

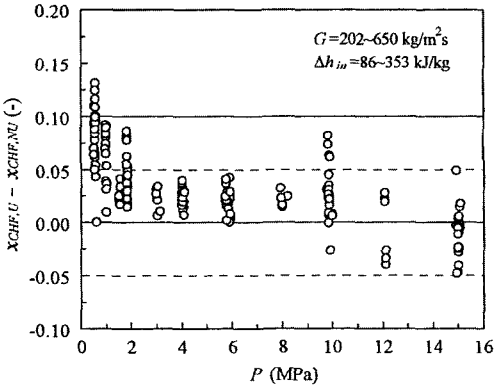

Fig. 15 Critical quality difference with pressure

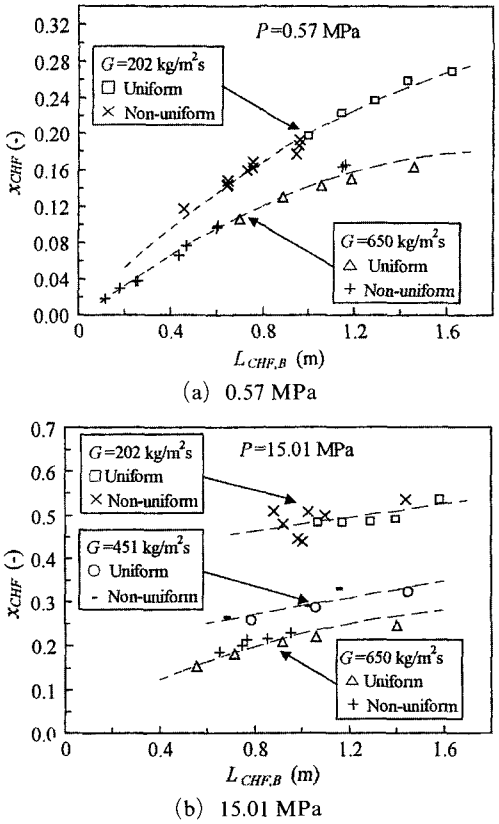

Fig. 16 Critical quality as a function of boiling length for pressure

where $q''_{CHF,avg,B}$, d_i and A_f are the average heat flux over the boiling length (from the saturation point to the CHF location), the heater rod diameter and the flow area, respectively. When the conditions of mass flux and pressure in the uniform and non-uniform heat flux data are equal, the following heat balance equation is obtained from Eq. (2):

$$\frac{x_{CHF,NU}}{L_{CHF,B,NU}} = \frac{q''_{CHF,avg,B,NU}}{q''_{CHF,avg,B,U}} \frac{x_{CHF,U}}{L_{CHF,B,U}} \tag{3}$$

The relationship of the parameters $x_{CHF,NU}/L_{CHF,B,NU}$ and $x_{CHF,U}/L_{CHF,B,U}$ with the same conditions (pressure, mass flux and inlet subcooling) is given in Fig. 17. This figure shows that the relationship between $x_{CHF,NU}/L_{CHF,B,NU}$ and $x_{CHF,U}/L_{CHF,B,U}$ keeps linearity over the entire range in the present experimental conditions. This signifies that the relationship between the boiling length and the critical quality in Fig. 16 holds good true throughout the entire range of pressure. Therefore, for high quality or annular flow conditions, the CHF can be calculated by the correlation based on the critical quality and boiling length, which is independent on the axial heat flux distribution, as follows:

$$x_{CHF} = f(d_o,\ d_i,\ L_h,\ L_{CHF,B},\ P,\ G) \tag{4}$$

In addition, when the CHF correlation with the form of Eq. (4) based on uniform heat flux data is applied to predict the CHF for non-uniform heating, the prediction results should satisfy the heat balance between the uniform and non-uniform data such as Eq. (3).

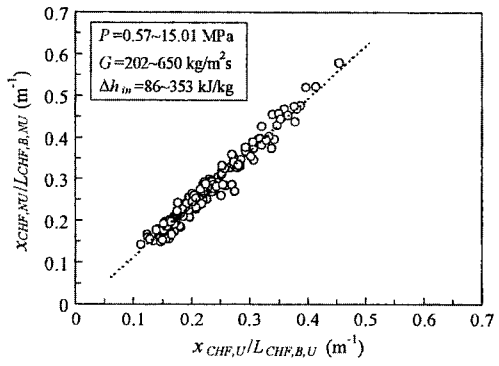

Fig. 17 Relationship between $x_{CHF,U}/L_{CHF,B,U}$ and $x_{CHF,NU}/L_{CHF,B,NU}$

4. Comparison with Existing Correlations

In the previous study (Chun et al., 2001), the CHF data for the uniform heat flux were compared with the existing CHF correlations and then the Doerffer et al. correlation (Doerffer et al., 1994) using the 1995 CHF look-up table (Groeneveld et al., 1996) and the Bowring correlation (Bowring, 1977) showed good prediction capabilities. Therefore, the CHF data obtained in the non-uniform heat flux experiments are compared with the Doerffer et al. correlation using the 1986 (Groeneveld et al., 1986) and 1995 look-up tables and the Bowring correlation.

Groeneveld et al. (1986) recommended the ratio of the boiling length average heat flux to the local heat flux at the CHF location as a an axial heat flux correction factor of the CHF look-up table:

$$K = \frac{q''_{CHF,avg,B}}{q''_{CHF,loc}} \quad \text{for } x_{CHF} > 0$$
$$K = 1 \quad \text{for } x_{CHF} \le 0 \tag{5}$$

The CHF value in the look-up table is multiplied by the correction factor, to modify the table value. In the Bowring correlation, the Y-parameter, which is defined as the ratio of the heat flux averaged from the bottom end of the heated section to the axial location Z to the local heat flux at the location Z in a practical application, is calculated as follows:

$$Y = \frac{\int_0^Z q''(z)\,dz}{q''(z)\,Z} \tag{6}$$

As shown in Fig. 18, the CHF is calculated as follows: Using assumed total power and given axial heat flux distribution, the local conditions such as local heat flux and local quality are calculated at each location Z that is divided into 100 locations from inlet to exit. By a preliminary study, the step size (18.42 mm) does not affect the CHF prediction results. Using the CHF correlations, the *local* CHF value is calculated at each location Z using the local conditions calculated above. If the local heat flux is equal to the *local*

CHF value, that is, the local critical heat flux ratio CHFR(z) (predicted *local* CHF/local heat flux) at any location is equal to a value of unity, it is judged that the CHF occurs at that point. If a minimum CHFR for the whole locations is not equal to a value of unity, then the total power to the test section is increased until the minimum CHFR is equal to a value of unity.

As shown in Fig. 19, the Doerffer et al. correlation shows relatively good prediction capability at pressures above 11 MPa. However, the correlation overestimates the *local critical power* at pressures below 11 MPa, and the overestimation becomes gradually large as the pressure decreases. The prediction error is particularly large at low pressures. The prediction capability of the Doerffer et al. correlation with the 1995 CHF look-up table is slightly better than that with the 1986 look-up table. Figure 20 shows the prediction results of the Bowring correlation. The results from the Bowring correlation show better prediction than those from the Doerffer et al. correlation with the 1995 CHF look-up table.

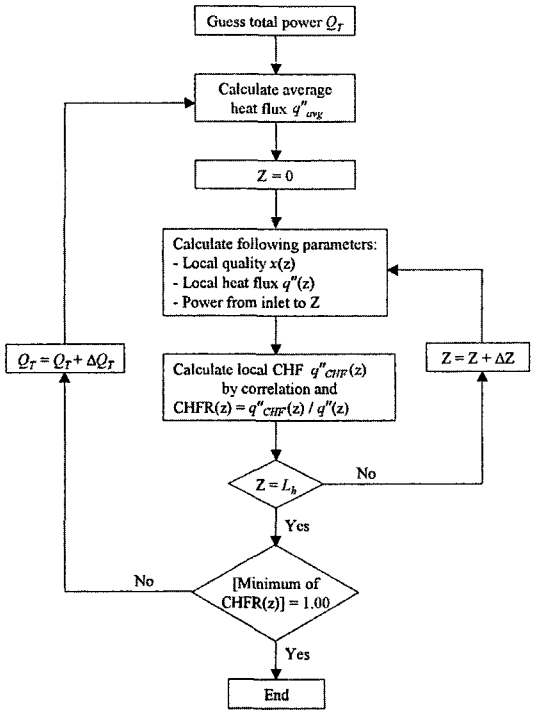

Fig. 18 CHF calculation procedure

The correlation has a tendency to overestimate the *local critical power* at pressures below 11 MPa and underestimate at high pressures above 13 MPa. Table 2 summarizes the CHF prediction

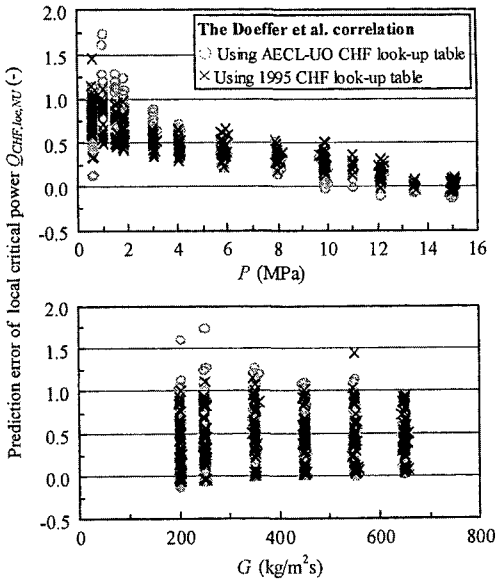

Fig. 19 Comparison of the present CHF data with the Doerfer et al. correlation
Prediction error
$= (Q_{CHF,loc,NU,cor} - Q_{CHF,loc,NU,exp}) / Q_{CHF,loc,NU,exp})$

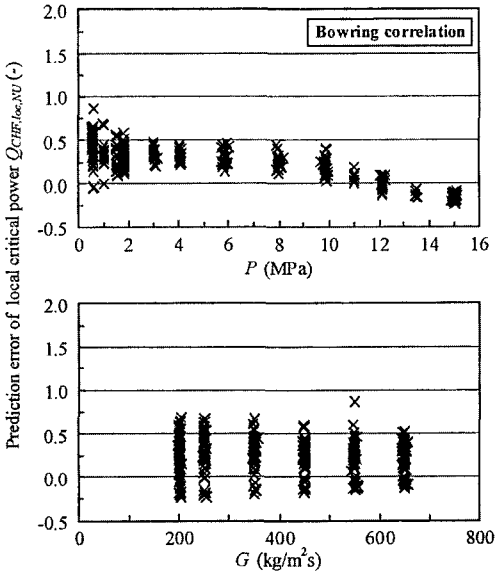

Fig. 20 Comparison of the present CHF data with the Bowring correlation

Table 2 CHF prediction results for non-uniform heating

Correlation	Mean error(%)	RMS error(%)
Doeffer et al. (using 1986 AECL-UO look-up table)	46. 1	58.0
Doeffer et al. (using 1995 look-up table)	45.1	53.8
Bowring	22.8	31.2

$$\text{Mean error}=\frac{1}{N}\sum_{i=1}^{N}[(Q_{CHF,loc,NU,cor}-Q_{CHF,loc,NU,exp})/Q_{CHF,loc,NU,exp}]\times 100$$

$$\text{RMS error}=\sqrt{\frac{1}{N}\sum_{i=1}^{N}[(Q_{CHF,loc,NU,cor}-Q_{CHF,loc,NU,exp})/Q_{CHF,loc,NU,exp}]^2}\times 100$$

results. The Doerffer et al. with the 1995 CHF look-up table and the Bowring correlations predicted the CHF data for uniform heat flux distribution within RMS error of 22.5% and 15.2%, respectively (Chun et al., 2001). When the Doerffer et al. and the Bowring correlations are applied for predicting CHF in the heated section with non-uniform axial heat flux distribution, the prediction results from these correlations have considerably large errors, compared with the prediction for uniform heat flux distribution.

5. Conclusions

CHF experiments have been conducted in an internally heated annulus with a chopped cosine heat flux distribution. In order to investigate the effect of non-uniform heating on CHF, the experimental conditions have been set at the same geometry and flow conditions as the uniform heat flux experiments. The following conclusions are obtained :

(1) The CHFs in the high pressure region above 10 MPa frequently occur at the top end of the heated section. In the present conditions, most of the CHFs occur in the annular flow regime and for the mechanism of the CHF, the liquid film dryout in annular flow is dominant.

(2) The *local* CHF with the parameters such as mass flux and critical quality shows an irregular behavior for the pressures of 0.57 and 15.01 MPa and deviates from a general trend that is represented by a unique curve, due to the unsteadiness of the CHF occurrence location. However, the *total critical power* with mass flux and the *average CHF* with critical quality can be approximately represented by a linear relationship without the irregularity for the whole pressure range in the present experimental conditions, respectively.

(3) The comparison between the uniform and the non-uniform heat flux data indicates that the effect of the heat flux distribution on CHF is large at low pressure conditions below 2 MPa. The values of the *total critical power* for the non-uniform heat flux agree with those for the uniform heat flux within an error of 10% at pressures above 2 MPa. This observation supports the 'overall power' hypothesis.

(4) For a fixed mass flux and pressure, the relationship between the critical quality and the boiling length is represented by a single curve, independent of the axial heat flux distribution, in the present experimental conditions.

(5) The Bowring correlation predicts CHF relatively better than the Doerffer et al. correlation. However, the prediction results from these correlations for non-uniform axial heat flux distribution have considerably large errors, compared to the prediction for uniform heat flux distribution.

Acknowledgment

The authors would like to thank the ministry of science and technology of Korea for their financial support of the Nuclear R & D Program.

References

ANSI/ASME PTC 19. 1, 1985, "ASME Performance Test Codes, Supplement on Instruments

and Apparatus, Part 1, Measurement Uncertainty," ASME.

Bergles, A. E., Collier, J. G., Delhaye, J. M., Hewitt, G. F. and Mayinger, F., 1981, "Two-Phase Flow and Heat Transfer in the Power and Process Industries," *Hemisphere Publishing corporation*, pp. 262~265.

Bowring, R. W., 1977, "A new Mixed Flow Cluster Dryout Correlation for Pressure in the Range 0.6-15.5 MN/m^2 (90-2250 psia) - for use in a Transient Blowdown Code," *Heat and Fluid Flow in Water Reactor Safety, Inst. of Mechanical Engineers*, pp. 175~182.

Chun, S. Y., Chung, H. J., Hong, S. D., Yang, S. K. and Chung, M. K., 2000, "Critical Heat Flux in Uniformly Heated Vertical Annulus Under a Wide Range of Pressures 0.57 to 15.0 MPa," *Journal of the Korean Nuclear Society*, Vol. 32, No. 2, pp. 128~141.

Chun, S. Y., Chung, H. J., Moon, S. K., Yang, S. K., Chung, M. K., Schoesse, T. and Aritomi, M., 2001, "Effect of Pressure on Critical Heat Flux in Uniformly Heated Vertical Annulus under low flow conditions," *Nucl. Eng. Des.*, Vol. 203, pp. 159~174.

Collier, J. G. and Thome, J. R., 1994, "Convective Boiling and Condensation, 3rd Edition," Oxford University Press, pp. 375~382.

Doerffer, S., Groeneveld, D. C., Chemg, S. C. and Rudzinski, K. F., 1994, "A Comparison of Critical Heat Flux in Tubes and Annuli," *Nucl. Eng. Des.*, Vol. 149, pp. 167~175.

El-Genk, M. S., Haynes, S. J. and Kim, S. H., 1988, "Experimental Studies of Critical Heat Flux for Low Flow of Water in Vertical Annuli at Near Atmospheric Pressure," *Int. J. Heat Mass Transfer*, Vol. 31, pp. 2291~2304.

Groeneveld, D. C., Cheng, S. C. and Doan, T., 1986, "1986 AECL-UO Critical Heat Flux Look-Up Table," *Heat Transfer Engineering*, Vol. 7 [1-2], pp. 46~62.

Groeneveld, D. C., Leung, K. H., Kirillov, P. L., Bobkov, V. P., Smogalev, I. P., Huang, X. C. and Royer, E., 1996, "The 1995 Look-Up Table for Critical Heat Flux in Tubes," *Nucl. Eng. Des.*, Vol. 163, pp. 1~23.

Mishima, K. and Ishii, M., 1982, "Experimental Study on Natural Convection Boiling Burnout in Annulus," *Proceeding of the 7th International Heat Transfer Conference*, Munchen, Vol. 4, pp. 309~314.

Mishima, M. and Nishihara, H., 1987, "Effect of Channel Geometry on Critical Heat Flux for Low Pressure Water," *Int. J. Heat Mass Transfer*, Vol. 30, pp. 1169~1182.

Park, J. W., Baek, W. P. and Chang, S. H., 1997, "Critical Heat Flux and Flow Pattern for Water Flow in Annular Geometry," *duddlNucl. Eng. Des.*, Vol. 172, pp. 137~155.

Rogers, J. T., Salcudean, M. and Tahir, A. E., 1982, "Flow Boiling Critical Heat Fluxes for Water in a Vertical Annulus at Low Pressure and Velocities," *Proceeding of the 7th International Heat Transfer Conference*, Munchen, Vol. 4, pp. 339~344.

Rosal, E. R., Cermak, J. O., Tong, L. S., Casterline, J. E., Kokolis, S. and Matzner, B., 1974, "High Pressure Rod Bundle DNB Data with Axially Non-Uniform Heat Flux," *Nucl. Eng. Des.*, Vol. 31, pp. 1~22.

Schoesse, T., Aritomi, M., Kataoka, Y., Lee, S. R., Yoshioka, Y. and Chung, M. K., 1997, "Critical Heat Flux in a Vertical Annulus Under Low Upward Flow and Near Atmospheric Pressure," *J. Nucl. Sci. Technol.*, Vol. 34, No. 6, pp. 559~570.

Todreas, N. E. and Rohsenow, W. M., 1966, "The Effect of Axial Heat Flux Distribution on Critical Heat Flux in Annular, Two Phase Flow," *Proceeding of the 3rd International Heat Transfer Conference*, Chicago, Vol. 3, pp. 78~85.

Tong, L. S., Currin, H. B., Larsen, P. S. and Smith, O. G., 1965, "Influence of Axially Non-Uniform Heat Flux on DNB," *AIChE Preprint 17, 8th National Heat Transfer Conference*, Los Angeles.

Tong, L. S., 1966, "Prediction of Departure From Nucleate Boiling for an Axially Non-Uniform Heat Flux Distribution," *Journal of Nuclear Energy*, Vol. 21, pp. 241-248.